Disintegration of uncertainties associated with real-time multi-satellite precipitation products in diverse topographic and climatic area in Pakistan

Muhammad MASOOD[1]* https://orcid.org/0000-0002-8072-2622; ✉e-mail: chmasoud@gmail.com

Ghulam NABI[1] https://orcid.org/0000-0002-1907-2798; e-mail: gnabi60@yahoo.com

Muhammad BABUR[2] https://orcid.org/0000-0003-3723-5674; e-mail: m.babur@ucp.edu.pk

Aftab Hussain AZHAR[3] https://orcid.org/0000-0001-7352-8584; e-mail: aftab_azharpk@yahoo.co.uk

Muhammad KALEEM ULLAH[4] https://orcid.org/0000-0003-3937-8337; e-mail: muhammad.kaleem1@ce.uol.edu.pk

* Corresponding author

1 Centre of Excellence in Water Resources Engineering, University of Engineering & Technology GT-Road, Lahore 54890, Pakistan

2 Civil Engineering Department, University of Central Punjab, Lahore 54782, Pakistan

3 Directorate of Hydrology, Pakistan Water & Power Development Authority (WAPDA), MDO-WAPDA, Mangla Dam 10200, Pakistan

4 Civil Engineering Department, University of Lahore, Lahore 54000, Pakistan

Abstract: Satellite-based Precipitation Estimates (SPEs) have gained importance due to enhanced spatial and temporal resolution, particularly in Indus basin, where raingauge network has fewer observation stations and drainage area is laying in many countries. Formulation of SPEs is based on indirect mechanism, therefore, assessment and correction of associated uncertainties is required. In the present study, disintegration of uncertainties associated with four prominent real time SPEs, IMERG, TMPA, CMORPH and PERSIANN has been conducted at grid level, regional scale, and summarized in terms of regions as well as whole study area basis. The bias has been disintegrated into hit, missed, false biases, and Root Mean Square Error (RMSE) into systematic and random errors. A comparison among gauge- and satellite- based precipitation estimates at annual scale, showed promising result, encouraging use of real time SPEs in the study area. On grid basis, at daily scale, from box plots, the median values of total bias (-0.5 to 0.5 mm) of the used SPEs were also encouraging although some under/over estimations were noted in terms of hit bias (-0.15 to 0.05 mm/day). Relatively higher values of missed (0.3 to 0.5 mm/day) and false (0.5 to 0.7 mm/day) biases were observed. The detected average daily RMSE, systematic errors, and random errors were also comparatively higher. Regional-scale spatial distribution of uncertainties revealed lower values of uncertainties in plain areas, depicting the better performance of satellite-based products in these areas. However, in areas of high altitude (>4000 m), due to complex topography and climatic conditions (orographic precipitation and glaciated peaks) higher values of biases and errors were observed. Topographic barriers and point scale gauge

data could also be a cause of poor performance of SPEs in these areas, where precipitation is more on ridges and less in valleys where gauge stations are usually located. Precipitation system's size and intensity can also be a reason of higher biases, because Microwave Imager underestimate precipitation in small systems (<200 km²) and overestimate in large systems (>2000 km²). At present, use of bias correction techniques at daily time scale is compulsory to utilize real time SPEs in estimation of floods in the study area. Inter comparison of satellite products indicated that IMERG gave better results than the others with the lowest values of systematic errors, missed and false biases.

Abbreviations:

IMERG: Integrated Multi-satellite Retrievals for Global Precipitation Measurement
CMORPH: Climate Prediction Center Morphing Technique
PERSIANN: Precipitation Estimation from Remotely Sensed Information using Artificial Neural Networks
GPM IMERG: Global Precipitation Measurement IMERG
SPEs: Satellite-Based Precipitation Estimates
TRMM: Tropical Rainfall Measuring Mission
CPC: Climate Prediction Center
DMSP: Defense Meteorological Satellite Program
PMD: Pakistan Meteorological Department
NOAA: National Oceanic and Atmospheric Administration
GPROF: Goddard Profiling
GPCC: Global Precipitation Climatology Centre
IMRT: IMERG Late real-time V5
TMPA: TMPA 3B42 real-time V7
CMOR: CMORPH (RAW) daily
PERS: PERSIANN daily near real-time

1 Introduction

The estimation of precipitation holds a key position in water resources assessment, planning and development. Because of significant temporal and spatial variability, estimation of precipitation is subjected to considerable uncertainty. Conventionally, rain gauges are used to measure the precipitation which is cost effective but with limited spatial representation. Development of precipitation radars facilitated the precipitation estimation process. The invention of Satellite-Based Precipitation Estimates (SPEs) further supplemented the precipitation estimation practices. The effective use of SPEs in remote locations and in the oceans has further increased their utilization (Kidd and Huffman 2011). Therefore, SPEs, as a substitute of gauge precipitation estimates, can also be utilized for drought assessment, flood estimation and hydrological modeling of sparsely gauged or ungauged watershed (Maggioni et al. 2016, Toté et al. 2015). The satellite-based precipitation estimation technology is based on an indirect approach, using infra-red and microwave spectrums of light and both these spectrums are required to improve the working of SPEs (Joyce et al. 2004). Hence, the application of SPEs needed validation before field application.

The performance of SPEs depends upon many factors such as land topography, climatic conditions, rainfall intensity, and patterns, etc. Consequently, the validation studies of SPEs are area specific. Studies have been conducted for assessment and validation of SPEs around the globe (Chen & Li 2016, Derin & Yilmaz 2014, Gao & Liu 2013, Gebremichael et al. 2010, Masood et al. 2018, Moazami et al. 2014, Prakash et al. 2018, Ringard et al. 2015, Sun et al. 2016, Tang et al. 2016, Zambrano-Bigiarini et al. 2017). These studies are based on the assessment of SPEs against gauge/radar data or intercomparison among various satellite products, where gauge/radar data were not available. Therefore, validation of SPEs using remote sensing means has been conducted several times (Dinku et al. 2007, Habib et al. 2009).

Due to the indirect mechanism of estimation in SPEs, there is a chance of inherited errors and associated uncertainties. Uncertainties in SPEs are from different factors, such as retrieval errors, sensor calibration, spatial and temporal sampling inaccuracies etc. (Hong et al. 2006, Boushaki et al. 2009). There can also be systematic errors, usually termed as biases (Hossain et al. 2006). Bias adjustment studies have been conducted in various areas using different approaches (Boushaki et al. 2009). Tobin and Bennett (2010) adjusted satellite precipitation data to remove false alarm or missed bias to facilitate hydrologic modeling. Muller and Thompson (2013) conducted bias adjustment of satellite rainfall data through stochastic modeling. Moazami et al. (2014) did uncertainty analysis of bias from satellite rainfall estimates using the Copula method. Cheema and Bastiaanssen (2012) adjusted

TRMM data using geographical differential analysis (GDA) and regression analysis (RA). Masood et al. (2018) introduced a new framework for the estimation of integrated satellite precipitation estimates (IFP), aimed at consistent performance throughout the study area.

Indus Basin River System is a constellation of transnational rivers contributed by flows from catchments lying in India, Nepal and China etc. , and it works as a lifeline to fulfill Pakistan's water requirements. In this area, precipitation does not occur throughout the year. It is associated with western disturbances, monsoon winds, and thunderstorms. Monsoon wind is the primary source of summer rainfall and 50% to 75% of rainfall is associated with it (Kazi and Khan 1951, Kureshy 1998). The main source of winter rainfall is the western disturbances (Khan 1993). Variation in monsoon rainfall can range from 17% to 59% (Luo and Lin 1999). More variation in monsoon rainfall has been observed than the thunderstorms and western disturbances. An increased variation in rainfall has also been observed from humid (northeast) to arid (south-west) areas at the Indus Basin (Kazi and Khan 1951). Hussain and Lee (2013, 2016) studied long term variability in inter-annual and summer monsoon rainfall in Pakistan and observed 20% to 65% variability across the study area. Under such varied climatic and topographic circumstances, collecting sparsely networked gauge observations from departments of various countries is an uphill task. Such precipitation data with the poor spatial representation of gauges can lead to incorrect data inputs in hydrological simulations.

SPEs have two major types - Real-Time and Research. Real-Time versions are utilized in flood forecasting, land sliding and disaster management. Research versions are customarily used for drought assessment, meteorological and climatological studies. The utilization of real-time SPEs has gained significant importance in this study area to avert losses from floods like those in 2010. In Pakistan, some studies have been conducted for assessment and validation of various SPEs (Anjum et al. 2018, Iqbal and Athar 2018, Khan et al. 2014). Until now, only Masood et al. (2019) have evaluated prominent real-time SPEs in this area. In addition to the assessment and validation, comprehensive error characterization of SPEs is needed for developments in retrieval processes, advancement of bias removal practices,

uncertainty models, and incorporation in other hydro-meteorological utilizations (AghaKouchak et al. 2009, Gebregiorgis and Hossain 2013).

Studies have been conducted for error characterization of satellite products in some parts of the world (AghaKouchak et al. 2012, Prakash et al. 2016). But according to Yong et al. (2016), error components of SPEs vary in different topographic and climatic regions. Hence, disintegration of uncertainties associated with SPEs in different climatic zones is necessary for users and developers. In this study error characterization of GPM IMERG real-time has been conducted in climatically and topographically diversified regions of Pakistan. For intercomparison, real-time versions of most widely used SPEs, TRMM, PERSIANN and CMORPH were used. The specific objectives of the study were to decompose total bias into hit, miss and false biases, and disintegrate associated errors into systematic and random errors and their spatial distribution over the study area. Being the first study in this area, it will provide valuable information not only to the users, but also to algorithm developers of real-time SPEs.

2　Materials and Methods

2.1 Study area

Pakistan extends approximately from 61° to 77° E (longitude) and 23.5° to 37° N (latitude) and demonstrates diverse climatic conditions. There exists significant variation in the topography of Pakistan. The altitude varies from sea-level (Arabian sea coastal line), with arid and warm climate in the south to chilling, snow-covered mountains towards north holding the tallest peaks with a height of around 7000 m, plain areas, deserts and plateaus in the center (Fig. 1). Because of varied climate, the precipitation, particularly the rainfall, varies considerably in space and time. Mean annual precipitation differs approximately from 300 mm to around 1800 mm from the south towards the north. Salma et al. (2012) studied precipitation patterns in various climatic regions of Pakistan, based on the analysis of 30 years of data. They classified the area of Pakistan into five regions based on average annual precipitation and other climatic parameters. Region A is in the north of Pakistan where weather is cold and exist tallest peaks, (34° to 38° N) in the Himalayan, Koh-Hindukash, and
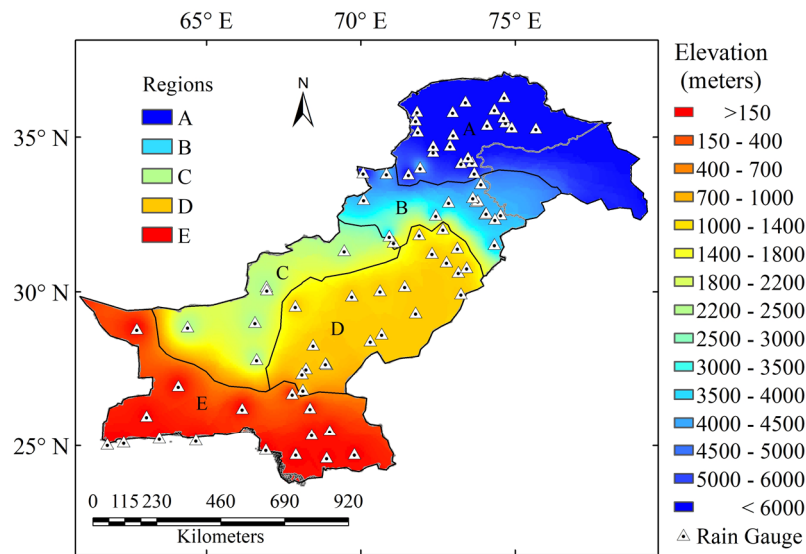
Fig. 1 Topography (elevation ranges in meters) of the study area, location of PMD's Rain Gauges (represented by Triangles) and regionalization of the study area (A, B, C, D, E) based on precipitation and elevation.

Kohe-Sufaid areas. The upper part of this region toward the north is glaciated and the lower part of the region has areas with the highest average annual rainfall (1800 mm). Region B is the transitional region between hilly and plain areas. This region has a slight cold environment and situated between 31° to 34° N. In some areas exists sub foothills and Pothohar Plateau. In region C, the weather is cold and temperature even drops below freezing point at some locations in winter. But summer is hot and the temperature reaches up to 40°C. It extends from 27° to 32° N and 64° to 70° E. There are also some hilly places having high altitudes above the mean sea level. Region D is the hottest, most dry part of the study area where highest temperatures (up to 53°C) have been reported. Most of the area in this region is plain, comprising irrigated agricultural lands and prominent deserts such as Thal, Cholistan, and Thar. Region E is a vast region, closer to the Arabian Sea. The coastline part covers only a small portion of the region and the weather of coastline area in the Balochistan and the Sindh province is almost dry to arid.

2.2 Rain gauge data

Pakistan Meteorological Department (PMD) has established more than one hundred meteorological stations across Pakistan to record metrological data (http://www.pmd.gov.pk/Observatories/index.html). Accumulated precipitation measurements are noted at 8:00 am daily. A few of these weather stations are operated occasionally under extreme weather conditions and therefore excluded from the analysis. Hence, eighty weather stations (represented by triangles) distrtubuted across all the regions of the study area (Fig. 1) were selected and accumulated daily precipitation in milli meters (mm) was used for disintegration of uncertainties associated with SPEs.

2.3 Satellite precipitation products

This study was aimed at the disintegration of uncertainties associated with high resolution multi-satellite real-time SPEs under varied climatic and topographic conditions in Pakistan. Four real-time SPEs used in this study are briefly described below (Masood et al. 2019).

2.3.1 Integrated multi-satellite retrievals for GPM (IMERG)

The GPM IMERG was launched in March, 2014. The IMERG is a (quasi-global) 60° N to 60° S "multi-satellite" based precipitation product (https://pmm.nasa.gov/GPM). Core observatory of GPM is equipped with two sensors: a 'GPM microwave imager (GMI)' that measures precipitation characteristics such as intensity, type, size and a 'Dual-frequency Precipitation Radar (DPR)' that observes internal structure of storm within and below the clouds (Kim et al. 2017). The algorithm used in IMERG formulation uses satellite retrievals from CMORPH of NOAA, TMPA of NASA, and PERSIANN (Liu 2015).

The input datasets are processed using GPROF, CPC Kalman-Filter with Lagrangian time interpolation and PERSIANN-CCS recalibration technique. GPM-IMERG is providing different types of data sets for end users, IMERG real-time and IMERG-research. IMERG- real-time has two types (i) 'Early real-time' released after 6 hours of observation (ii) 'Late real-time' provided about 18 hours after observation. These products are usually recommended for landslides and flood warnings. After receiving gauge observations and calibration against the GPCC's gauge data, the IMERG Research product is generated approximately 3-months after the observation. These products include precipitation, with a $0.1° \times 0.1°$ spatial resolution and temporal resolution of 30-minutes (Tang et al. 2016, Chen et al. 2016, Yuan et al. 2017). In the present study daily IMERG Late real-time V5, hereafter 'IMRT' was used for error characterization and comparison with other prominent real-time SPEs.

2.3.2 Tropical Rainfall Measuring Mission (TRMM)

The TRMM (https://pmm.nasa.gov/data-access/downloads/trmm) is a joint venture of National Space Development Agency of Japan, and NASA launched it in 1997. It was planned for research and monitoring of tropical, subtropical precipitation and energy emissions. Widely used TRMM products include TCI-TRMM Combined Calibration database (TRMM 2B31), TRMM Multi-Satellite Precipitation Analysis (TMPA 3B42 and 3B43). The algorithm of TMPA was designed by NASA's Goddard Space Flight Centre (GSFC). TRMM 3B42 V7 has been produced using data from the passive microwave observations, making use of the Goddard Profiling (GPROF) 2010 algorithm and generating Geo-Infrared precipitation estimates using the best values from the GPROF. The 3B42 and 3B43 are usually available at monthly average, daily and sub-daily average, at a spatial resolution of $0.25° \times 0.25°$ with a quasi-global scale of (50°N to 50°S). In this study, TMPA 3B42 real-time V7, hereafter 'TMPA' was used for the disintegration of associated uncertainties and comparison with IMERG and other real-time SPEs.

2.3.3 CPC Morphing Technique (CMORPH)

CMORPH is a high-resolution global precipitation product at a spatial resolution of $0.25° \times 0.25°$ and a temporal resolution of 3 hours.

The original CMORPH version is called Version 0.x, and the reprocessed CMORPH version is called Version 1.0. Version 1.0 has three products: (i) RAW (CMORPH-RAW), (ii) a bias-corrected product (CMORPH-CRT), and (iii) a gauge-satellite blended product (CMORPH-BLD). The CMORPH-RAW product is a satellite-only precipitation product. CMORPH-RAW uses precipitation approximations derived from low orbiting microwave satellite observations only, whose characteristics are conveyed via spatial broadcast data, obtained entirely from geostationary Infra-Red satellite (http:/ftp.cpc.ncep.noaa.gov/precip/global_CMORPH/). Each file contains binary records; (a) holds the combined microwave precipitation and (b) the "CMORPH" precipitation approximations in millimeters per hour. Missing records are represented by "-9999". The CMORPH (RAW), hereafter 'CMOR' daily, similar to real-time in IMERG and TRMM was used in this study.

2.3.4 PERSIANN

"Precipitation Estimation from Remotely Sensed Information using Artificial Neural Networks (PERSIANN)" is formulated by "Center for Hydrometeorology and Remote Sensing" (CHRS) University of California Irvine (http://chrsdata.eng.uci.edu/). It uses neural network classification to estimate precipitation rate, at spatial resolution of $0.25° \times 0.25°$. The PERSIANN scheme depends upon geostationary infrared images strengthened with the use of infrared and daytime imageries together. The system uses gridded infrared images of global geosynchronous satellites (GOES-8, GOES-10, GMS-5, Metsat-6, and Metsat-7) provided by CPC, NOAA to generate 30-minute precipitation rates. Parameters are regularly updated using precipitation estimates from low orbiting satellites, including TRMM, NOAA-15, -16, -17, DMSP F13, F14, F15. Precipitation product covers 60° S to 60° N on a global scale. PERSIANN daily near real-time data, hereafter 'PERS' was used in this study.

2.4 Extraction of satellite data

In order to characterize the uncertainties associated with the satellite-based precipitation products the tiles of selected SPEs at daily time scale in '.tif' format, having an end time approximately the same as that of measurement at PMD precipitation gauges (from 3:00 to 3:00 UTC to match with the

PMD local gauge observation time 8:00 to 8:00), were downloaded from March 2014 till September 2017. In several data integration schemes, the ways used to handle weather station data (point values) have limitations. Normally such schemes are focused on downscaling of grid-scale data and upscale interpolation of point values. Consequently, the gridded data differ from the station observations in numerous aspects (Ciach & Krajewski 1999, Li & Heap 2008, Nešpor & Sevruk 1999, Scheel et al. 2011). In order to avoid such in-accuracies (downscaling and upscale interpolation) a more rational technique was proposed and applied (Hu et al. 2016, Ward et al. 2011). In this technique, precipitations measured at stations lying within a grid cell were averaged to get an estimate for the measured precipitation at the center of that grid cell for comparison with gridded data. This method was used in this study for point to pixel comparison. Daily precipitation data of eighty gauging stations lying across the study area was obtained from the PMD. The unit of precipitation of both gauges and the SPEs was daily accumulated rainfall in millimeters (mm/day).

2.5 Characterization of uncertainties

Uncertainties associated with SPEs are due to observing sensors, algorithms involved in transforming observations into precipitation estimates, and sampling errors. These uncertainties can be classified into biases and errors. Since only a set of finite number of observations is sampled from the actual population of precipitation events, errors mainly depend upon the sampling design of sensors, and biases are due to systematic problems (Huffman 1997). Bias is usually defined as the average difference between the values of satellite estimate and rain gauge measured values. It can be positive or negative. Positive bias represents over-estimation, while negative bias stands for under-estimation. It is usually decomposed into three types, hit, missed, and false biases (Tian et al. 2009). Total bias was computed using Eq.(1).

$$\text{Bias} = \frac{\sum_{i=1}^{N}(P_{Si}-P_{Oi})}{N} \qquad (1)$$

where P_{Si} represents the satellite estimate, P_{Oi} the gauge observation in the respective pixel, and N stands for the sample size. Contribution of hit bias, missed bias, and false bias toward total bias is computed using Eq. (2) (Tian et al. 2009).

$$\text{Bias} = \text{Hit} - \text{Miss} + \text{False} \qquad (2)$$

Hit bias is the accumulated difference in millimeters per unit time between the precipitation recognized both by the satellite and gauge at a certain place. Missed bias is the accumulated amount of precipitation in millimeters per unit time at a particular location when rain gauge reported precipitation, but the satellite reported no precipitation. False bias is the accumulated value in millimeters at a specific site per unit time when rain gauge reported no precipitation, but the satellite reported precipitation.

The root means square error (RMSE) is used to represent the average magnitude of the error. It gives higher weight to the larger errors relative to mean absolute errors. A value of RMSE equal to zero means that there is no error between the estimated and the observed data and the magnitude of error increases with increasing RMSE. It was computed using Eq. (3).

$$\text{RMSE} = \left[\frac{\sum_{i=1}^{N}(P_{Si}-P_{Oi})^2}{N}\right]^{1/2} \qquad (3)$$

RMSE was decomposed into Random errors and Systematic errors using Eq. (4) (Prakash et al. 2016).

$$\text{RMSE} = \text{Systematic}_{err} + \text{Random}_{err} \qquad (4)$$

Systematic and random errors were computed using Eqs. (5) and (6) respectively (AghaKouchak et al. 2012).

$$(\text{RMSE})_{sys} = \sqrt{\frac{\sum_{i=1}^{n}(P_{si}^{*}-P_{oi})^2}{N}} \qquad (5)$$

$$(\text{RMSE})_{rand} = \sqrt{\frac{\sum_{i=1}^{n}(P_{si}-P_{si}^{*})^2}{N}} \qquad (6)$$

P^{*}_{Si} was computed using a linear regression error model, Eq.(7).

$$P_{si}^{*} = a \times R_{oi} + b \qquad (7)$$

where 'a' is the slope and 'b' is the intercept. The regression model was developed for each of the four SPEs, and RMSE was decomposed into systematic and random errors.

3 Results

In this study, an inside view of uncertainties associated with high resolution, real-time multi-satellite SPEs was carried out over an area having diverse topographic and climatic conditions by disintegration of bias and RMSE. This characterization of uncertainties is essential for the development of effective bias reduction techniques to

refine precipitation retrieval algorithms and for operational utilization of SPEs in such areas. Some evaluation studies of different SPEs in this area have shown correlation coefficient (CC) values up to 0.9 at a monthly scale (Anjum et al. 2018) and up to 0.6 at a daily scale (Masood et al. 2019) etc. To have an outlook of performance of SPEs in the study area, average annual precipitation values given by the selected SPEs, and that of the PMD rain gauges were plotted for the selected period of time (Fig. 2) (Masood et al. 2019).

It was found that all the SPEs successfully captured from North to South decreasing trend in average annual precipitation in the study area, although some underestimation was observed. The spatially distributed underestimation contrast among SPEs and PMD data was further widened in parts of regions A and B. Significant variation was observed at locations situated in the lower parts of region A and upper parts of region B, where the terrain is hilly, and average annual precipitation is relatively higher. Some portion of region B consists of 'Pothohar' area where the terrain is undulated, but the average annual precipitation is relatively lower than the lower parts of

Fig. 2 Spatial distribution of average annual precipitation of the used SPEs and PMD's rain gauge data.

region A. Comparatively more resemblance in spatial distribution patterns of average annual precipitation by SPEs and rain gauges were observed in plain areas. The average annual trend of IMRT had a relatively higher resemblance with that of the gauge data. The resemblance in spatially distributed precipitation patterns reduced further between PMD and TMPA which was further reduced in CMOR and PERS.

3.1 Overall disintegration of uncertainties

In order to have an overall insight of uncertainties associated with the used SPEs in the study area, box plots of statistical indices - Bias, hit bias, missed bias, false bias, RMSE, systematic errors, and random errors were plotted against reference (rain gauge) data (Fig. 3). Usually, box plots are considered very helpful in depicting performance, when two or more datasets are compared based upon a large number of observations. Box plot generates information in terms of a five-number summary, very beneficial in descriptive analysis, or the initial analysis of large data sets. The summary contains five ranges: the most extreme values in the data set (the highest and lowest values also referred as upper and lower limits), the first and third quartiles, and the median value. All these values are presented together and ordered from lowest to highest: minimum value, first quartile, median value, third quartile, and maximum value.

It was observed that the median value of total bias of the selected SPEs was in the range of -0.5 to 0.5 mm per day and that of the first & third quartiles were in the range of -1 to 3.5 mm per day. Product-wise values of total bias in term of the first and third quartile were, TMPA (-1 to 2.5 mm/day), PERS (-1 to 3 mm/day), IMRT (-1.5 to 3 mm/day) and CMOR (-0.5 to 3.5 mm/day) against PMD rain gauge data. On an average, the results of the total averaged daily bias in mm revealed the effectiveness of the selected SPEs toward the estimation of precipitation. The median values of hit bias were found in the range of 0 to -0.15, showing underestimation in the values of estimated precipitation. CMOR exhibited overall the lowest values of hit bias against PMD gauge data. Based on the hit bias results of the first and third quartile, CMOR also revealed relatively better performance, among the selected SPEs, followed by IMRT, TMPA, and PERS, respectively. Significant values of missed biases were observed in the estimation of
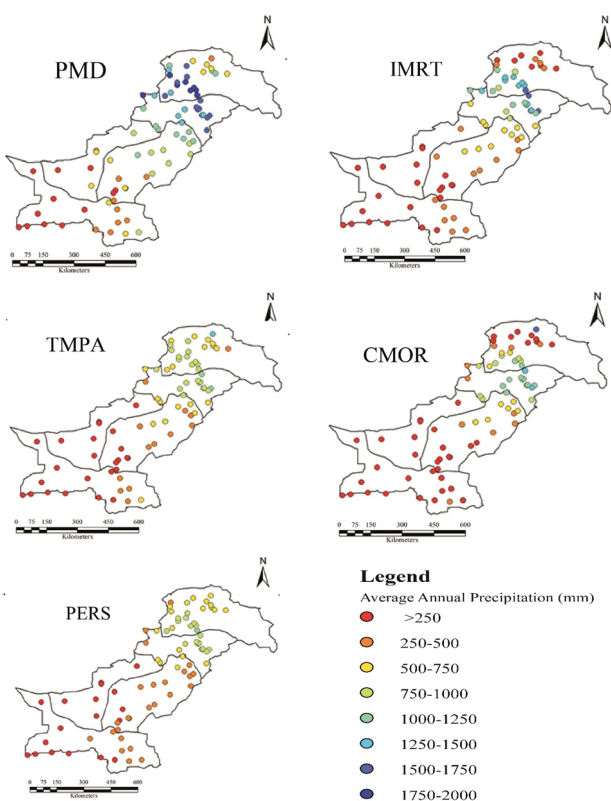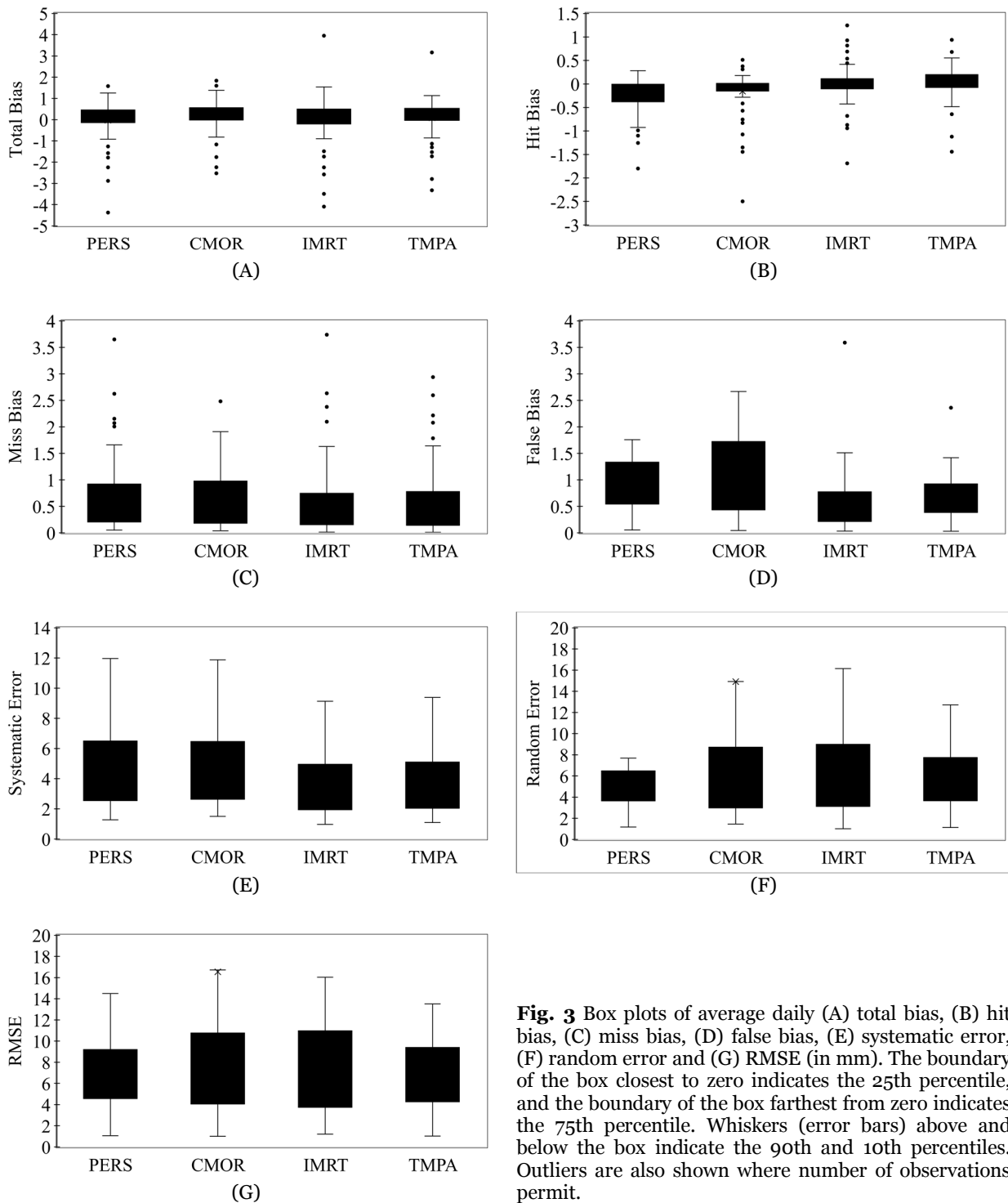
Fig. 3 Box plots of average daily (A) total bias, (B) hit bias, (C) miss bias, (D) false bias, (E) systematic error, (F) random error and (G) RMSE (in mm). The boundary of the box closest to zero indicates the 25th percentile, and the boundary of the box farthest from zero indicates the 75th percentile. Whiskers (error bars) above and below the box indicate the 90th and 10th percentiles. Outliers are also shown where number of observations permit.

precipitation by SPEs. Median values of missed precipitation in the study area were in the range of 0.3 to 0.5 mm for the used SPEs. The results of the first and third quartile of missed biases showed that IMRT (0.2 to 0.6 mm/day) performed relatively better among the selected SPEs followed by TMPA (0.2 to

0.7 mm/day), PERS (0.2 to 0.75 mm/day) and CMOR (0.2 to 0.9 mm/day). The box plot revealed that all the used SPEs have false biases in the estimated precipitation. It was also observed that the magnitude of false bias was relatively larger as compared to the missed and hit biases in the study area. Median values

of average daily false bias were in the range of 0.5 to 0.7 mm. IMRT showed the least median value of false bias. Based on the results of the first and third quartile of false bias the IMRT (0.3 to 0.7 mm/day) gave relatively better results followed by TMPA (0.4 to 0.75 mm/day), PERS (0.5 to 1.3 mm/day) and CMOR (0.45 to 1.7 mm/day).

Median values of RMSE were observed in the range of 6 to 7.5 mm per day and that of the first and third quartile were in the range of 4 to 11 mm per day. Based on the median value of RMSE, PERS exhibited relatively better results followed by IMRT, TMPA, and CMOR. The RMSE results of the first and third quartile revealed a bit identical ranges of the selected SPEs depicting, PERS (4.5 to 8.5 mm/day), IMRT (3.5 to 10 mm/day), TMPA (5 to 8 mm/day) and CMOR (4 to 11 mm/day). In the case of systematic errors, the average daily values were found in the range of 3 to 4 mm and that of the first and third quartile were found in the range of 2 to 6.7 mm per day. In terms of systematic errors the SPEs can be arranged as IMRT (2 to 4.7 mm/day), TMPA (2.1 to 4.8 mm/day), PERS (2.2 to 6.7 mm/day), and CMOR (2.25 to 6.6 mm/day). The IMRT gave relatively lower values of systematic errors, followed by TMPA, PERS, and CMOR. The median values of averaged daily random errors of the selected SPEs ranged from 4.5 to 6 mm. The first and third quartile values were in the range of 3 to 8 mm per day. Based on the results of the first and the third quartile of random errors, SPEs can be ranked as PERS (3.5 to 6 mm/day), TMPA (4 to 5 mm/day), IMRT, and CMOR (3 to 8 mm/day), respectively.

3.2 Spatially distributed disintegration of uncertainties

In order to have a look at spatial distribution of uncertainties associated with the used high-resolution real-time multi-satellite SPEs, the study area was divided into five regions (Fig. 1), based on climatic and topographic conditions. The daily averaged values of total bias of the used SPEs were observed in the range of -0.15 to 0.15 (Fig. 4(A)). It was also noted that the highest values of underestimations against reference data were found at locations in the lower part of region A, a hilly terrain having maximum average annual rainfall (up to 1800 mm) in the study area and overestimation was found at locations in region B, a foothill area, joining mountainous region with the plain area. In the rest of the study area, especially in plain areas of regions D and E, the used

SPEs showed lower values of total average daily Bias. Overall trend of the total bias exhibited by IMRT was identical with CMOR and that of TMPA was alike PERS. TMPA and PERS produced relatively lower overestimation as compared to IMRT and CMOR in region B but comparatively overestimated the total bias in the glaciated upper part of region A.

Spatial distribution of hit bias of the used real-time SPEs (Fig. 4(B)) was identical with total bias but its magnitude was relatively less as compared to the total bias. The highest values of underestimation were produced at locations in lower parts of the region A by all the used SPEs. Though overestimation at some locations in the upper glaciated part of region A and locations in region B was expressed by IMRT and TMPA, only the PERS underestimated the bias both in region B and the lower part of region A.

The spatial distribution of missed bias revealed that the highest value of missed precipitation was observed at locations in the lower part of region A, and at some points in adjacent foothill region B (Fig. 4(C)). A decrease in the magnitude of missed precipitation was observed from the north toward south, a pattern identical with the distribution of average annual rainfall in the study area (Fig. 2). In terms of false bias the most challenging locations for Real-time SPEs were also in the lower part of region A, and in region B, Fig. 4(D), where higher values of false bias against reference data were observed. North to south decreasing trend was also observed in the value of false bias. IMRT and TMPA gave relatively lesser values of false bias as compared to CMOR and PERS. Larger values of averaged daily RMSE up to 15 mm were observed for the selected real-time SPEs (Fig. 5(A)). Relatively higher values of RMSE were found at locations in the lower part of the hilly terrain of region A, and in the foothill of region B. Magnitude of RMSE was reduced comparatively at locations in plain areas of region D and E towards the southwest. The selected SPEs, showed relatively lower values of systematic errors as compared to RMSE (Fig. 5(B)). It was found that the magnitude of systematic errors at locations in hilly topography of region A and region B was higher as compared to the rest of the study area. The value of systematic error was reduced in plain areas of regions D and E, and its magnitude also reduced further toward the southwest. The spatial distribution of random errors against reference data of used SPEs across the study area (Fig. 5(C)), revealed that lower values of random errors were observed in plain areas.
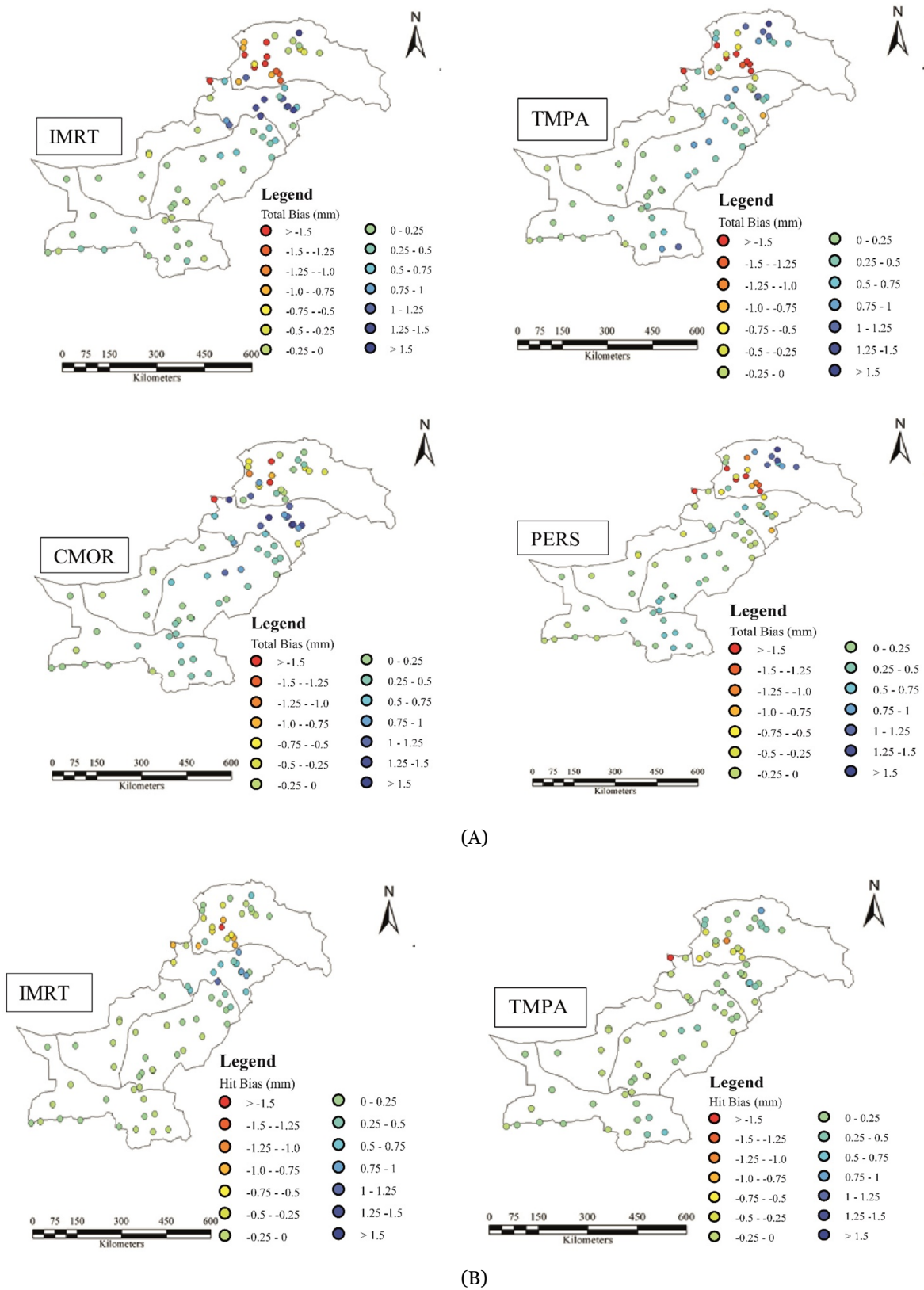
(A)

(B)

Fig. 4 Spatial distribution of averaged daily (A) total bias, (B) hit bias, (C) missed bias and (D) false bias (in mm) for the selected real time satellite products.
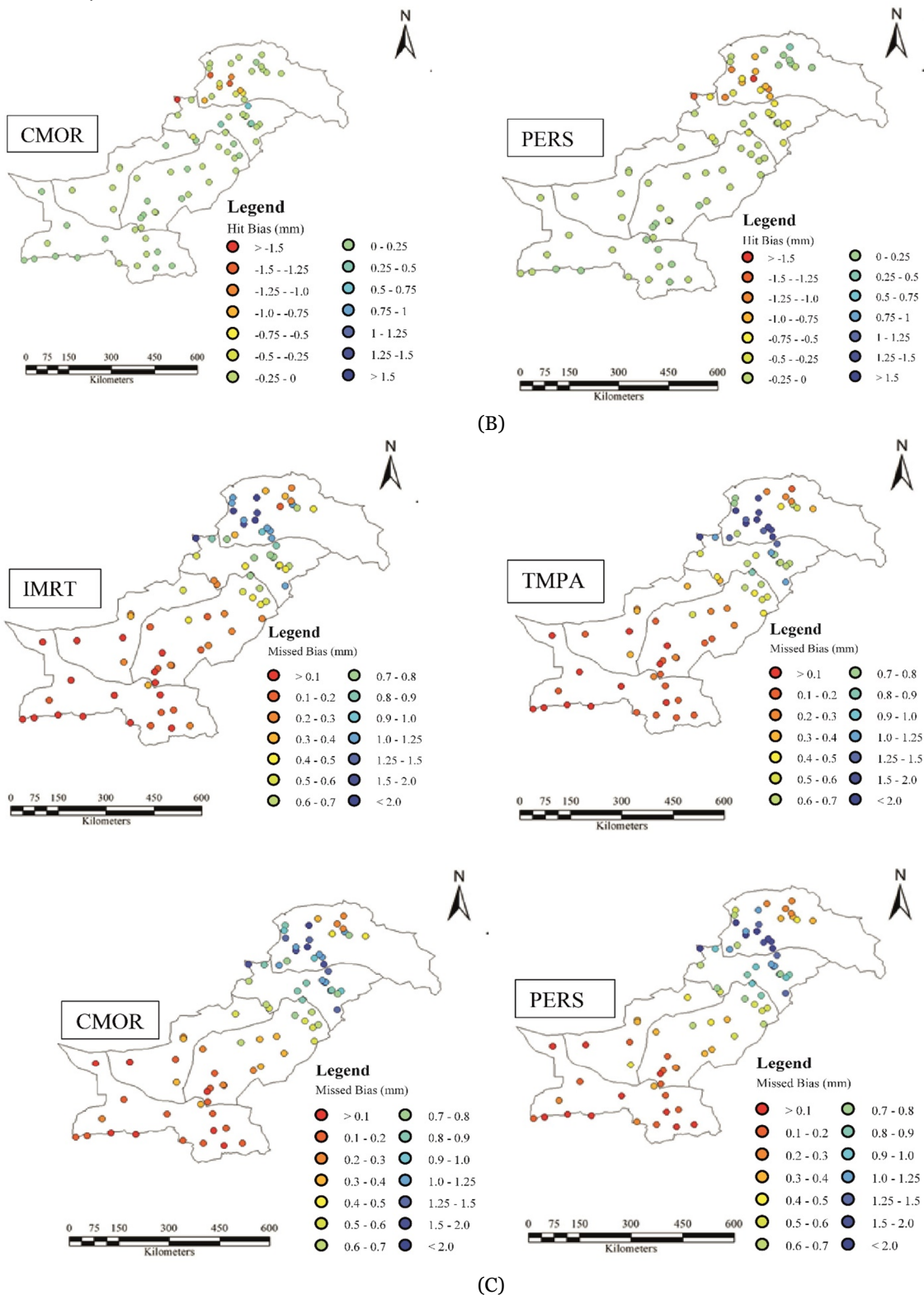
(-To be continued-)

(-Continued-)

(B)

(C)

Fig. 4 Spatial distribution of averaged daily (A) total bias, (B) hit bias, (C) missed bias and (D) false bias (in mm) for the selected real time satellite products.
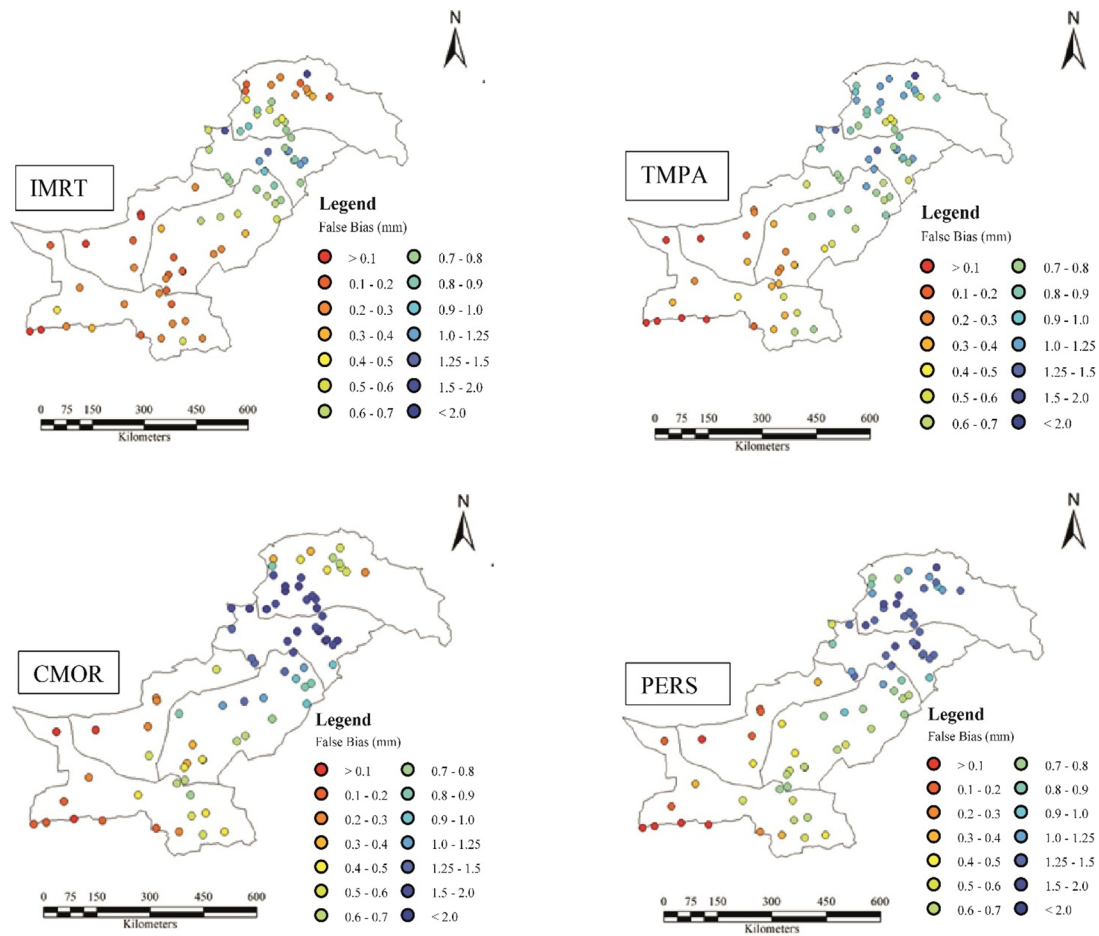(-To be continued-)

(-Continued-)

(D)

Fig. 4 Spatial distribution of averaged daily (A) total bias, (B) hit bias, (C) missed bias and (D) false bias (in mm) for the selected real time satellite products.

Comparatively higher values of random errors were observed at stations in hilly areas, comprising the lower part of region A and region B. It was noted that higher values of errors (RMSE, Random, and Systematic) were observed at places in region B and lower parts of region A.

3.3 Summarized regional disintegration of uncertainties

In order to have a concise understanding of the accompanying uncertainties and intercomparison of performance of the selected real-time SPEs, averaged daily values upon regional (five regions) and entire study area basis of total bias, its components (hit bias, missed bias, false bias), RMSE, systematic and random errors were plotted (Fig. 6).

The results of averaged daily total bias (Fig. 6(A)), revealed underestimation in the assessment of precipitation by all the used SPEs in regions A and C as compared to PMD rain gauge data. The highest magnitude of underestimation was observed in regions A and that of overestimation was found in region B.
In region C, the terrain is also hilly, but lower values of bias may be due to lower average annual rainfall. The value of bias was further reduced in plain regions D and E. The results of hit bias (Fig. 6(B)), revealed that all the selected SPEs overestimated precipitation in regions B, D & E and underestimated the precipitation in regions A and C. Highest values of overestimations were observed in region B, and highest values of underestimations were found in region A. It is evident from the results of hit bias that most challenging areas for application of SPEs are
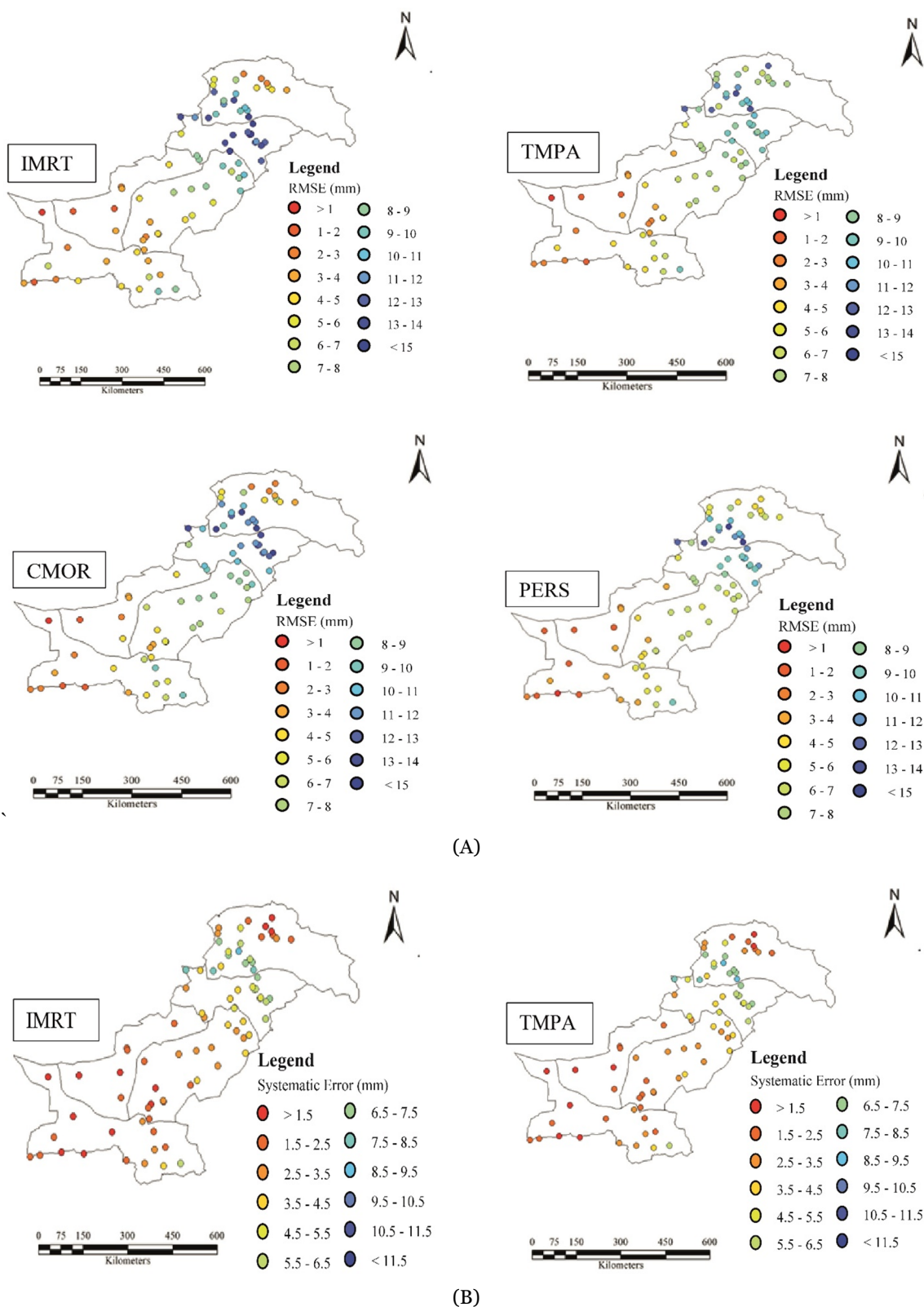
Fig. 5 Spatial distribution of averaged daily (A) Root means square error, (B) Systematic error and (C) Random error (in mm).
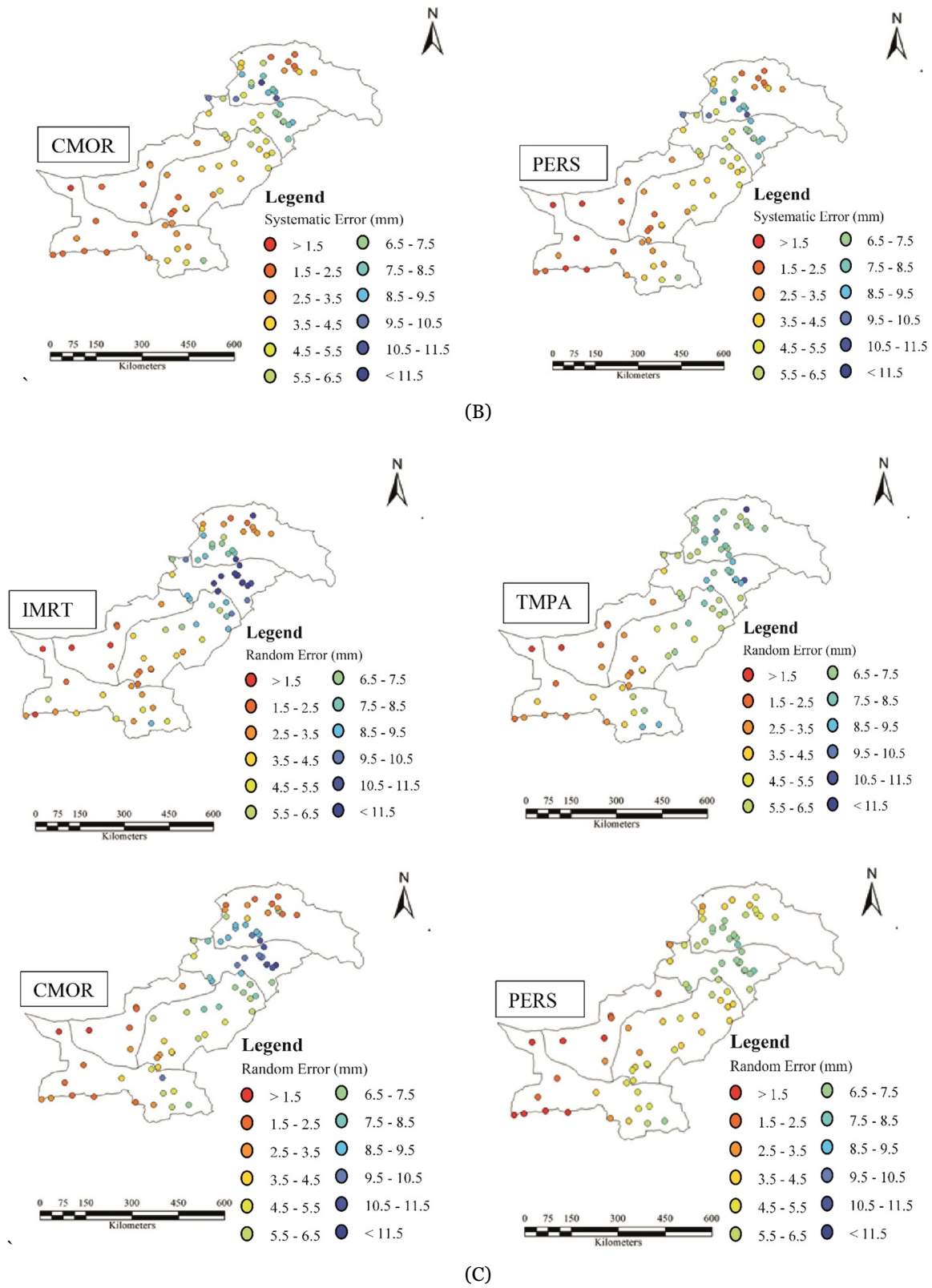
(-To be continued-)

(-Continued-)

(B)

(C)

Fig. 5 Spatial distribution of averaged daily (A) Root means square error, (B) Systematic error and (C) Random error (in mm).

region A and B. The results of missed Bias (Fig. 6(C)) revealed that all the four real-time SPEs has a significant share of missed bias contributing towards the total bias on the regional as well as the entire study area basis. It was also observed that the highest values of missed precipitation were exhibited by the selected SPEs in Region A and B. Summarized results

of false bias based on the entire study area and regional basis (Fig. 6(D)), showed that the selected real-time SPEs revealed higher values of average daily false bias in regions A and B relative to other regions.
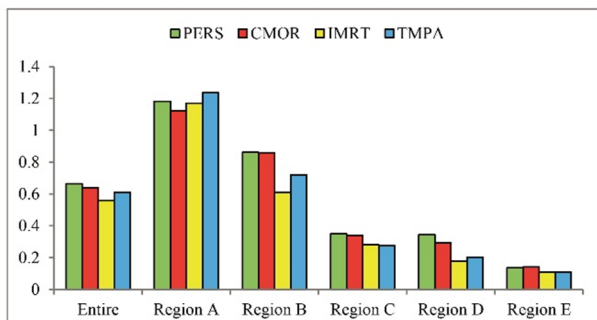
The averaged daily values of RMSE up to 11 millimeters were observed at regional and entire study area basis (Fig. 6(E)). The highest values of
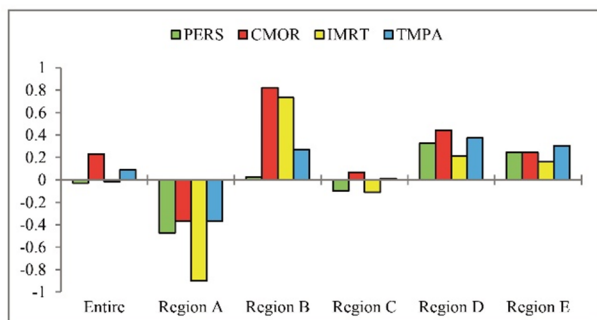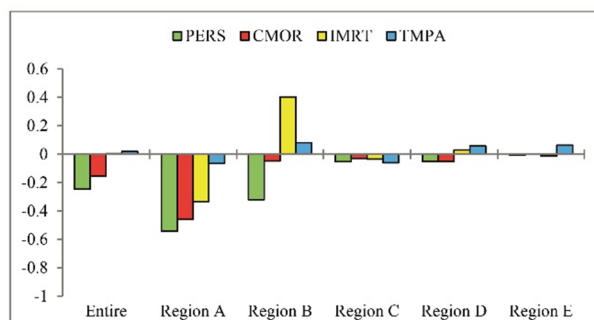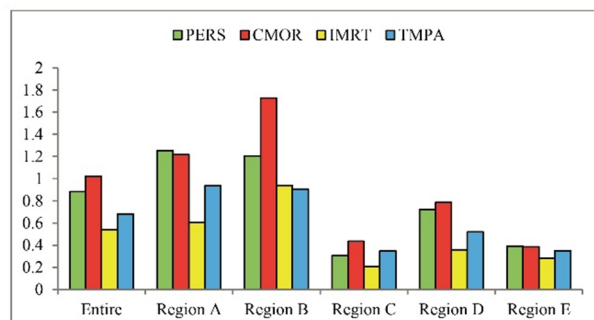
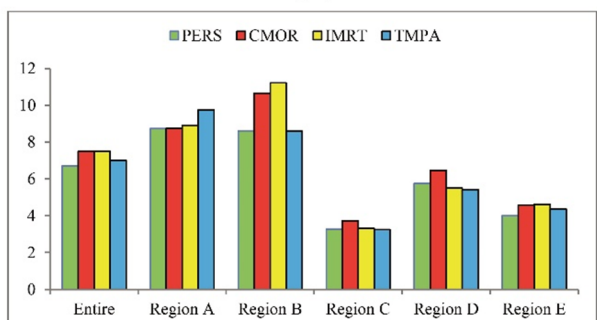
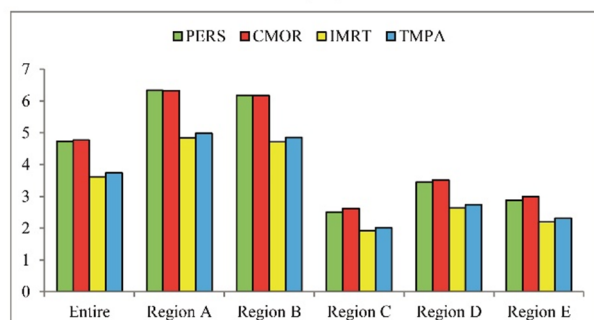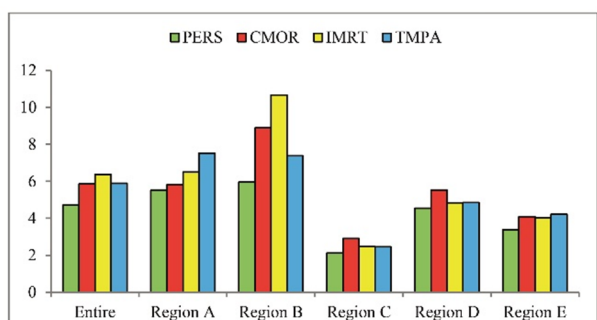
Fig. 6 Averaged daily values of (A) total bias, (B) hit bias, (C) missed bias, (D) false bias, (E) Root means square error, (F) systematic and (G) random errors (in mm) based on regional and the entire study area.

RMSE against reference data were also observed in regions A and B as compared to other regions. The magnitude of RMSE was reduced in plain areas of regions D, and E. The average daily values of systematic errors were observed in the range of 2 to 6 mm (Fig. 6(F)). Comparatively higher values of systematic errors were found in regions A and B. The average daily values of random errors ranged from 2 to 11 mm (Fig. 6(G)). Higher values of random errors were produced in regions A and B by the selected SPEs. Intercomparison among the selected SPEs showed that PERS exhibited relatively lower values of random errors on the entire study area as well as a regional basis.

4 Discussion

There are four seasons in Pakistan. About 50% of the area is arid, 40% is semi-arid and only 10% area (sub-Himalayas and Himalayas) of the total area is humid (Shirazi et al. 2006, Naqvi and Rehmat 1962, Khan 2002). Satellite-based precipitation estimates have enhanced their utility in the hydrological simulation due to finer, spatial and temporal resolutions. As the satellite-based precipitation estimates are obtained from reflected levels of energy using remote sensing tools, all such products need validation when they are used for practical application purposes (Masood et al. 2018, Moazami et al. 2014, Prakash et al. 2018). Due to the indirect formulation mechanism, there are chances of inherited uncertainties associated with these products. Hence, disintegration of uncertainties and correction techniques are needed for the precise application of such products (Prakash et al. 2016, Ringard et al. 2015). According to Yong et al. (2016), error mechanisms of SPEs vary in different topographic and climatic regions. In this study area, some validation studies of various SPEs has been conducted (Ali et al. 2017, Masood et al. 2018, Anjum et al. 2018, Iqbal et al. 2018, Masood et al. 2019). But up till now, not even a single study has been conducted to disintegrate uncertainties associated with real-time SPEs for the Indus basin.

The overall characterization of bias in terms of box plots of the used SPEs revealed encouraging median values of averaged daily total bias though some under/over estimation was found in terms of hit bias. The major share in total bias was contributed from missed and false biases. In the disintegration of

RMSE into random and systematic errors, it was noted that the magnitude of random errors was more as compared to systematic errors, identical with the findings of Prakash et al. (2015). AghaKouchak et al. (2012) observed that the retrieval algorithms of some SPEs do not use spatially homogeneous data sets and hence do not have uniform error characterization. It revealed that sensors and corresponding algorithms need further improvement. It was found that the latest product IMRT, using dual-frequency precipitation radar (DPR) showed lowest values of systematic errors, missed and false biases among the used SPEs, but still need to reduce random errors.

Spatially distributed results of uncertainties revealed that the most challenging areas with reference to the performance of SPEs were mountainous regions (lower part of region A and region B) where highest magnitudes of biases and errors were observed. The lower part of region A covers the Pir Panjal range (lesser Himalayas), Muree hills (sub-Himalayas), and adjacent Galliat. The direction of the sub-Himalayas and the Lesser Himalayas is east to west along with the Great Himalayas. The elevation of this region varies between 1500 m to 5000 m from south to north. This region is also the wettest part of the country and receives rainfall both in winter and summer seasons. Winter rains come due to western disturbances, a few thunderstorms in summer, and the monsoon from the Bay of Bengal. The topographical barrier such as Margalla hills, Murree hills, and Pir Panjal range receive high rainfall on southern slopes in monsoon season in terms of orographic precipitation. The region B is of belt shape, running along part of the Pir Panjal foothills and the Potwar plateau towards the eastern border with India. The direction of the Pir Panjal range is east to west north. Southeasterly monsoon moves along the Pir Panjal range and breaks against the topographic barrier such as Margalla hills and Salt range. The direction of the Salt range and Margalla hills is from north to south. The elevation of the Salt range and Margalla hills is 1122 m and 1580 m, respectively. Salt range and Margalla hills act as a barrier and break the strength of monsoon, in result high rainfall at Margalla hills and Salt range. This region is the neighboring region of the lower part of region A, known as the highest rainfall region in the study area.

According to Wang et al. (2020), the utilization of SPEs in the area with elevation more than 2500m

demonstrated considerable limitations due to reduced quantitative capability of the DPR algorithm for solid precipitation. Adhikari et al. (2019) studied performance of Microwave Imagers (MI) in estimating the preipitation and found that MI underestimate the precipitation volume in warm and small system (size < 200 km²) while overestimate in larger system (size > 2000 km²). Maggioni et. al (2016) also reported higher values of uncertainties in SPEs with higher magnitude and intensities of precipitation. In the orographic regions diverse topography, complex microphysical processes and scale interactions lead to larger errors in SPEs (Palazzi et al. 2013, Prakash et al. 2015). According to Hence et al. (2012), the size and shape of a hill or mountain has a significant influence on the eventual spreading of precipitation in the area and is assessed by a combination of the thermodynamics of moist air, microphysics of particle growth and the dynamical behavior of a fluid flow encountering a terrain barrier. Therefore, deep convective systems arising near mountains precipitate when low-level flow bump into hills near the bases of key mountain ranges. In frontal cloud systems precipitating of the cloud is of maximum level over the first rise of topography. In such areas, higher values of biases and errors are due to poor identification between precipitating and non-precipitating cloud based on top infra-red temperature of the cloud (Dinku et al. 2010, Gebregiorgis & Hossain 2013, Hirpa et al. 2010).

Summarized results of the disintegration of uncertainties also revealed that mountainous regions (A & B) are the most challenging areas for the utilization of SPEs. In glaciated areas of region A, the poor performance of precipitation products may be due to lack of distinction between temperature and emissivity of rough land surfaces (i.e., water and snow-covered area). The generated background signals may be identical to those generated by precipitation, producing misinterpretation amid rainy or not rainy clouds. It might produce large bias in precipitation estimates in glaciated areas (Ferraro et al. 2000, Hussain et al. 2017, Satgé et al. 2016, Tian et al. 2007). Therefore, such areas need further investigation for the precise application of satellite-based precipitation products.

5 Conclusions

SPEs have gained recognition due to enhanced spatial and temporal resolution over conventional precipitation measuring approaches using gauges and radars. Their effective use is further aggravated in areas like Pakistan where the basin of the main riverine system - the Indus basin is laying in many countries like Pakistan, China, India etc. where conventional gauging system is sparse due to hilly topography. To secure reliable precipitation data from such locations falling in various countries for effective hydrological modeling is an uphill task. Since formulation mechanism of SPEs is based on recordings of reflectance using remote sensing tools, validation, identification and correction of associated uncertainties is required. In the present study, disintegration of uncertainties associated with four prominent real time SPEs has been conducted for their effective utilization in flood modeling to avert losses from 2010 like floods in the study area.

Overall characterization using box plots, the median values of bias of used real time products encouraged that the SPEs can be utilized in the study area to supplement the conventional precipitation gauging system. However, significant magnitude of false and missed biases was also observed and in total bias major share was contributed from these two biases. In the disintegration of RMSE into random and systematic errors, magnitude of random errors was more as compared to systematic errors.

Region wise disintegration of uncertainties revealed that the most challenging areas for application of SPEs were hilly glaciated terrains (upper part of region A), areas with highest average annual rainfall (lower part of region A and region B). In such areas precipitation is most on ridges and least in valleys. Conventionally, gauging stations are established in valleys. That is why underestimation in the lower part of region A and overestimation in region B was found with reference to gauge data. From the summarized results, on the entire study area and the regional basis, it was also found that all the four real-time SPEs has a significant share of missed and false biases contributing towards the total bias and highest values of these biases were exhibited by the selected SPEs in Region A and B. The highest averaged daily values of RMSE, systematic and random errors at regional and entire study area basis against reference data were also found in regions A and B as compared to other regions. The magnitude of errors was reduced in plain areas of region D, and E.

An inter comparison among the selected SPEs

revealed that IMRT showed relatively lower values of biases followed by TMPA, PERS, and CMOR. The results of RMSE and random errors showed a close contest between PERS and IMRT. IMRT also demonstrated lowest value of systematic errors reflecting that the latest product in this clan, whose formulation is based upon the modern capturing and updated processing algorithms. It was noted that all the four SPEs revealed higher values of Missed and False biases and need bias correction before application in hydrologic applications. It is evident that further investigation in retrieval algorithms is necessary in formulation of real time SPEs because compared with research SPEs, no bias corrections has been conducted using ground data. The disintegration of Bias and RMSE demonstrated three regions of the study area based upon the performance of SPEs: a) plain areas with lower to moderate rainfall, b) Hilly areas with higher rainfall intensities, C) Glaciated hilly areas. A future study to investigate the performance of these SPEs in these regions keeping in view the retrieval algorithms will be of significant value for developers of these products.

Acknowledgment

References

Adhikari A, Liu CT, Hayden L (2019) Uncertainties of GPM Microwave Imager Precipitation Estimates Related to Precipitation System Size and Intensity. J of Hydrometeor 20: 1907-1923. https://doi.org/10.1175/JHM-D-19-0038.1.

AghaKouchak A, Mehran A, Norouzi H, et al. (2012) Systematic and random error components in satellite precipitation data sets. Geophys Res Lett 39(9): L09406. https://doi.org/10.1029/2012GL051592

AghaKouchak A, Nasrollahi N, Habib E (2009) Accounting for uncertainties of the TRMM satellite estimates. Remote Sens 1(3): 606-619. https://doi.org/10.3390/rs1030606

Anjum MN, Ding YJ, Shangguan DH, et al. (2018) Performance evaluation of latest integrated multi-satellite retrievals for Global Precipitation Measurement (IMERG) over the northern highlands of Pakistan. Atmos Res 205: 134-146. https://doi.org/ 10.1016/j.atmosres.2018.02.010

Boushaki FI, Hsu K, Sorooshian S, et al. (2009) Bias adjustment of satellite precipitation estimation using ground-based measurement: A case study evaluation over the southwestern United States. J Hydrometeorol 10(5): 1231-1242. https://doi.org/10.1175/2009JHM1099.1

Cheema MJM, Bastiaanssen WG (2012) Local calibration of remotely sensed rainfall from the TRMM satellite for different periods and spatial scales in the Indus Basin. Int J Remote Sens 33(8): 2603-2627. https://doi.org/10.1080/01431161.2011.617397

Chen F, Li X (2016) Evaluation of IMERG and TRMM 3B43 monthly precipitation products over mainland China. Remote Sens 8(6): 472. https://doi.org/10.3390/rs8060472

Ciach GJ, Krajewski WF (1999) On the estimation of radar rainfall error variance. Adv Water Resour 22(6): 585-595. https://doi.org/10.1016/S0309-1708(98)00043-8

Derin Y, Yilmaz KK (2014) Evaluation of multiple satellite-based precipitation products over complex topography. J Hydrometeorol 15(4): 1498-1516. https://doi.org/10.1175/JHM-D-13-0191.1

Dinku T, Ceccato P, Grover-Kopec E, et al. (2007). Validation of satellite rainfall products over East Africa's complex topography. Int J Remote Sens 28(7): 1503-1526. https://doi.org/10.1080/01431160600954688

Dinku T, Ruiz F, Connor SJ, et al. (2010) Validation and intercomparison of satellite rainfall estimates over Colombia. J Appl Meteorol Climatol 49(5): 1004-1014. https://doi.org/10.1175/2009JAMC2260.1

Ferraro RR, Weng FZ, Grody NC, et al. (2000) Precipitation characteristics over land from the NOAA-15 AMSU sensor. Geophys Res Lett 27(17): 2669-2672. https://doi.org/10.1029/2000GL011665

Gao YC, Liu MF (2013) Evaluation of high-resolution satellite precipitation products using rain gauge observations over the Tibetan Plateau. Hydrol Earth Syst Sci 17(2): 837. https://doi.org/10.5194/hess-17-837-2013

Gebregiorgis A, Hossain F (2013) Performance evaluation of merged satellite rainfall products based on spatial and seasonal signatures of hydrologic predictability. Atmos Res 132: 223-238. https://doi.org/10.1016/j.atmosres.2013.05.003

Gebregiorgis AS, Hossain F (2013) Estimation of satellite rainfall error variance using readily available geophysical features. IEEE Trans Geosci Remote Sens 52(1): 288-304. https://doi.org/10.1109/TGRS.2013.2238636

Gebremichael M, Anagnostou EN, Bitew MM (2010) Critical Steps for Continuing Advancement of Satellite Rainfall Applications for Surface Hydrology in the Nile River Basin 1. J Am Water Resour Assoc 46(2): 361-366. https://doi.org/10.1111/j.1752-1688.2010.00428.x

Habib E, Larson BF, Graschel J (2009) Validation of NEXRAD multisensor precipitation estimates using an experimental dense rain gauge network in south Louisiana. J Hydrol 373(3-4): 463-478. https://doi.org/10.1016/j.jhydrol.2009.05.010

Hence DA, Houze Jr RA (2012) Vertical structure of tropical cyclones with concentric eyewalls as seen by the TRMM Precipitation Radar. J Atmos Sci 69(3): 1021-1036. https://doi.org/10.1175/JAS-D-11-0119.1

Hirpa FA, Gebremichael M, Hopson T (2010) Evaluation of high-resolution satellite precipitation products over very complex terrain in Ethiopia. J Appl Meteorol Climatol 49(5): 1044-1051. https://doi.org/10.1175/2009JAMC2298.1

Hong Y, Hsu Kl, Moradkhani H (2006) Uncertainty quantification of satellite precipitation estimation and Monte Carlo assessment of the error propagation into hydrologic response. Water Resour Res 42(8). https://doi.org/10.1029/2005WR004398

Huffman GJ (1997) Estimates of root-mean-square random error for finite samples of estimated precipitation. J Appl Meteorol Climatol 36(9): 1191-1201. https://doi.org/10.1175/1520-0450(1997)036<1191:EORMSR>2.0.CO;2

Hu ZY, Hu Q, Zhang C, et al. (2016) Evaluation of reanalysis, spatially interpolated and satellite remotely sensed precipitation data sets in central Asia. J Geophys Res 121(10): 5648-5663. https://doi.org/10.1002/2016JD024781

Hussain S, Song XF, Ren GY, et al. (2017) Evaluation of gridded precipitation data in the Hindu Kush–Karakoram–Himalaya mountainous area. Hydrol Sci J 62(14): 2393-2405. https://doi.org/10.1080/02626667.2017.1384548

Hussain MS, Lee S (2013) The regional and the seasonal variability of extreme precipitation trends in Pakistan. Asia-Pac J Atmos Sci 49(4): 421-441. https://doi.org /10.1007/s13143-013-0039-5

Hussain MS, Lee S (2016) Investigation of summer monsoon rainfall variability in Pakistan. Meteorol Atmos Phys 128(4): 465-475. https:// doi.org /10.1007/s00703-015-0423-z

Hossain F, Anagnostou EN, Bagtzoglou AC, (2006) On Latin Hypercube sampling for efficient uncertainty estimation of satellite rainfall observations in flood prediction. Comput Geosci 32(6): 776-792. https:// doi.org /10.1016/j.cageo.2005.10.006

Iqbal MF, Athar H (2018) Validation of satellite based precipitation over diverse topography of Pakistan. Atmos Res 201: 247-260. https:// doi.org /10.1016/j.atmosres.2017.10.026

Joyce RJ, Janowiak JE, Arkin PA, et al. (2004) CMORPH: A method that produces global precipitation estimates from passive microwave and infrared data at high spatial and temporal resolution. J Hydrometeorol 5(3): 487-503. https://doi.org/10.1175/1525-7541(2004)005<0487:CAMTPG>2.0.CO;2

Kazi S, Khan M (1951) Variability of rainfall and its bearing on agriculture in the arid and semi-arid zones of West Pakistan. Pak Geogr Rev 6(1): 40-63.

Khan FK (2002) Pakistan Geography. Economy and People, New Edition, (Ameena Saiyid, Oxford University Press, Korangi, Karachi, 2008), 1-199.

Khan JA (1993) The climate of Pakistan. Rehbar Publishers Karachi. pp 10-70.

Khan SI, Hong Y, Gourley JJ, et al. (2014) Evaluation of three high-resolution satellite precipitation estimates: Potential for monsoon monitoring over Pakistan. Adv Space Res 54(4): 670-684. https://doi.org/10.1016/j.asr.2014.04.017

Kim S, Hong S, Joh M, et al. (2017) Deeprain: Convlstm network for precipitation prediction using multichannel radar data. In: Proceedings of the 7th International Worksop on Climate Informatics, 20-22 September 2017. Bibcode: 2017arXiv171102316K

Kidd C, Huffman G (2011) Global precipitation measurement. Meteorol Appl 18(3): 334-353. https://doi.org/10.1002/met.284

Li J, Heap AD (2008) A review of spatial interpolation methods for environmental scientists. Geoscience Australia, Record 2008/23. pp 4-25.

Liu JZ, Duan Z, Jiang JC, et al. (2015) Evaluation of three satellite precipitation products TRMM 3B42, CMORPH, and PERSIANN over a subtropical watershed in China. Adv Meteorol Volume 2015, Article ID 151239. https://doi.org/10.1155/2015/151239

Luo QY, Lin E (1999) Agricultural vulnerability and adaptation in developing countries: the Asia-Pacific region. Clim Change 43(4): 729-743. https://doi.org/10.1023/A:1005501517713

Maggioni V, Meyers PC, Robinson MD (2016) A review of merged high-resolution satellite precipitation product accuracy during the Tropical Rainfall Measuring Mission (TRMM) era. J Hydrometeorol 17(4): 1101-1117. https://doi.org/10.1175/JHM-D-15-0190.1

Masood M, Shakir AS, Waseem M, et al. (2018) Integrated framework For Assessment of Blended High-Resolution Satellite Rainfall Estimates Over Complex Environmental Regions. Fresenius Environ Bull 27(12 B): 9747-9754.

Masood M, Shakir AS, Azhar AH, et al. (2019) Assessment of Real Time, Multi-Satellite Precipitation Products under Diverse Climatic and Topographic Conditions. Asia-Pac. J Atmos Sci 56: 577-591. https://doi.org/10.1007/s13143-019-00166-1

Moazami S, Golian S, Kavianpour MR, et al. (2014) Uncertainty analysis of bias from satellite rainfall estimates using copula method. Atmos Res 137: 145-166. https://doi.org/10.1016/j.atmosres.2013.08.016

Naqvi S, Rehmat M (1962) Weather and climate of Pakistan. Pak Geogr Rev 17: 12-16.

Moazami S, Golian S, Hong Y, et al. (2016) Comprehensive evaluation of four high-resolution satellite precipitation products under diverse climate conditions in Iran. Hydrol Sci J 61(2): 420-440. https://doi.org/10.1080/02626667.2014.987675

Müller MF, Thompson SE (2013) Bias adjustment of satellite rainfall data through stochastic modeling: Methods development and application to Nepal. Adv Water Resour 60: 121-134. https://doi.org/10.1016/j.advwatres.2013.08.004

Nešpor V, Sevruk B (1999) Estimation of wind-induced error of rainfall gauge measurements using a numerical simulation. J Atmos Ocean Technol 16(4): 450-464. https://doi.org/10.1175/1520-0426(1999)016<0450:EOWIEO>2.0.CO;2

Prakash S, Mitra AK, AghaKouchak A, et al. (2018) A preliminary assessment of GPM-based multi-satellite precipitation estimates over a monsoon dominated region. J Hydrol 556: 865-876. https://doi.org/: 10.1016/j.jhydrol.2016.01.029

Prakash S, Mitra AK, Rajagopal E, et al. (2016) Assessment of TRMM - based TMPA - 3B42 and GSMaP precipitation products over India for the peak southwest monsoon season. Int J Climatol 36(4): 1614-1631. https://doi.org/10.1002/joc.4446

Prakash S, MitraAK, AghaKouchak A, et al. (2015) Error characterization of TRMM Multisatellite Precipitation Analysis (TMPA-3B42) products over India for different seasons. J Hydrol 529: 1302-1312. https://doi.org/10.1016/j.jhydrol.2015.08.062

Prakash S, Mitra AK, Momin IM, et al. (2015) Comparison of TMPA-3B42 versions 6 and 7 precipitation products with gauge-based data over India for the southwest monsoon period. J Hydrometeorol 16(1): 346-362. https://doi.org/10.1175/JHM-D-14-0024.1

Palazzi E, Von Hardenberg J, Provenzale A (2013) Precipitation in the Hindu - Kush Karakoram Himalaya: observations and future scenarios. J Geophys Res 118(1): 85-100. https://doi.org/10.1029/2012JD018697

Ringard J, Becker M, Seyler F, et al. (2015) Temporal and spatial assessment of four satellite rainfall estimates over French Guiana and North Brazil. Remote Sens 7(12): 16441-16459. https://doi.org/10.3390/rs71215831

Salma S, Rehman S, Shah M (2012) Rainfall trends in different climate zones of Pakistan. Pak J Meteorol 9(17).

Satgé F, Bonnet MP, Gosset M, et al. (2016) Assessment of satellite rainfall products over the Andean plateau. Atmos Res 167: 1-14. https://doi.org/10.1016/j.atmosres.2015.07.012

Scheel M, Rohrer M, Huggel C, et al. (2011) Evaluation of TRMM Multi-satellite Precipitation Analysis (TMPA) performance in the Central Andes region and its dependency on spatial and temporal resolution. Hydrol Earth Syst Sci 15(8): 2649-2663. https://doi.org/10.5194/hess-15-2649-2011.

Sun RC, Yuan HL, Liu XL, et al. (2016) Evaluation of the latest satellite–gauge precipitation products and their hydrologic applications over the Huaihe River basin. J Hydrol 536: 302-319. https://doi.org/10.1016/j.jhydrol.2016.02.054

Tang GQ, Zeng ZY, Long D, et al. (2016) Statistical and hydrological comparisons between TRMM and GPM level-3 products over a midlatitude basin: Is day-1 IMERG a good successor for TMPA 3B42V7? J Hydrometeorol 17(1): 121-137. https://doi.org/10.1175/JHM-D-15-0059.1

Tian YD, Peters-Lidard CD, Choudhury BJ, et al. (2007) Multitemporal analysis of TRMM-based satellite precipitation products for land data assimilation applications. J Hydrometeorol 8(6): 1165-1183. https://doi.org/10.1175/2007JHM859.1

Tian YD, Peters - Lidard CD, Eylander JB, et al. (2009) Component analysis of errors in satellite - based precipitation estimates. J Geophys Res Atmos 114(D24). https://doi.org/10.1029/2009JD011949

Tobin KJ, Bennett ME (2010) Adjusting satellite precipitation data to facilitate hydrologic modeling. J Hydrometeorol 11(4): 966-978. https://doi.org/10.1175/2010JHM1206.1

Toté C, Patricio D, Boogaard H, et al. (2015) Evaluation of satellite rainfall estimates for drought and flood monitoring in Mozambique. Remote Sens 7(2): 1758-1776. https://doi.org/10.3390/rs70201758

Wang MH, Shi W, Watanabe S (2020) Satellite-measured water properties in high altitude Lake Tahoe. Water Res 115839. https://doi.org/10.1016/j.watres.2020.115839

Ward E, Buytaert W, Peaver L, et al. (2011) Evaluation of precipitation products over complex mountainous terrain: A water resources perspective. Adv Water Resour 34(10): 1222-1231. https://doi.org/10.1016/j.advwatres.2011.05.007

Yong B, Chen B, Tian YD, et al. (2016) Error-component analysis of TRMM-based multi-satellite precipitation estimates over mainland China. Remote Sens 8(5): 440. https://doi.org/10.3390/rs8050440

Yuan F, Zhang LM, Win KWW, et al. (2017) Assessment of GPM and TRMM multi-satellite precipitation products in streamflow simulations in a data-sparse mountainous watershed in Myanmar. Remote Sens 9(3): 302. https://doi.org/10.3390/rs9030302

Zambrano-Bigiarini M, Nauditt A, Birkel C, et al. (2017) Temporal and spatial evaluation of satellite-based rainfall estimates across the complex topographical and climatic gradients of Chile. Hydrol Earth Syst Sci 21(2): 1295. https://doi.org/10.5194/hess-21-1295-2017